BIOCHEMISTRY
including biophysical chemistry & molecular biology

Article

pubs.acs.org/biochemistry

Analysis of Diffuse K^+ and Mg^{2+} Ion Binding to a Two-Base-Pair Kissing Complex by Single-Molecule Mechanical Unfolding

Pan T. X. Li*

Department of Biological Sciences and The RNA Institute, University at Albany, SUNY, Albany, New York 12222, United States

Supporting Information

ABSTRACT: The folding and stability of RNA tertiary interactions depend critically on cationic conditions. It is usually difficult, however, to isolate such effects on tertiary interactions from those on the entire RNA. By manipulating conformations of single RNA molecules using optical tweezers, we distinguished individual steps of breaking and forming of a two-base-pair kissing interaction from those of secondary folding. The binding of metal ions to the small tertiary structure appeared to be saturable with an apparent K_d of 160 mM for K^+ and 1.5 mM for Mg^{2+}. The kissing formation was estimated to be associated with binding of ~2−3 diffuse K^+ or Mg^{2+} ions. At their saturated binding, Mg^{2+} provided ~3 kcal/mol more stabilizing energy to the structure than K^+. Furthermore, the cations change the unkissing forces significantly more than the kissing ones. For example, the presence of Mg^{2+} ions increased the average unkissing force from 21 pN to 44 pN, surprisingly high for breaking merely two base pairs; in contrast, the mean kissing force was changed by only 4.5 pN. Interestingly, the differential salt effects on the transition forces were not caused by different changes in the height of the kinetic barriers but were instead attributed to how different molecular structures respond to the applied force. Our results showed the importance of diffuse cation binding to the stability of tertiary interaction and demonstrated the utility of mechanical unfolding in studying tertiary interactions.

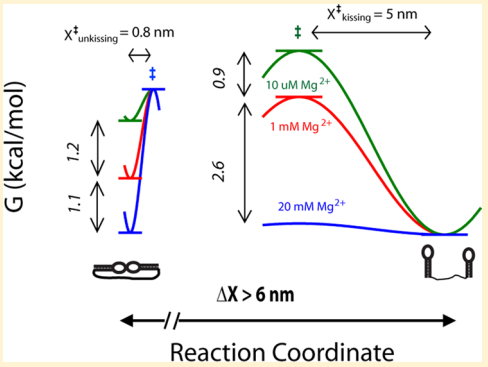

RNA tertiary folding critically depends on cationic conditions, particularly the concentration of divalent cations such as Mg^{2+}.[1−6] This strong ionic dependence partially arises from structural compaction during tertiary formation, resulting in a high density of negative charges on phosphate groups that need to be offset by cations. As biological functions of RNA molecules depend on their proper folding, cations play vital roles in many molecular processes essential for life. For example, Mg^{2+} ion is indispensable for tertiary folding and function of tRNAs,[7,8] ribozymes,[9−11] riboswitches,[12−14] and ribosomes.[15−17] However, neither tertiary folding nor its dependence on cations can be reliably predicted. There is no equivalent of the nearest neighbor parameters used for secondary structure prediction.[18,19] Cationic effects on tertiary interactions have to be studied case by case, taking into account the structure and shape of the RNA of interest. A general and thermodynamically rigorous interpretation of the role of cations in stabilizing RNA tertiary structure, as well as more experimental studies on tertiary folding, is still needed.

As increasing cation concentration stabilizes global RNA structure, it is often difficult to experimentally distinguish the stabilizing effects on secondary and tertiary structures. Moreover, cations display a range of thermodynamically distinct activities, ranging from the binding of fully dehydrated ions to specific sites[20−23] to the diffusive associations that shell an RNA surface.[24−27] In addition, Mg^{2+} ions compete with monovalent cations for binding to RNA.[28,29] Binding of cations to tertiary structures in complex RNAs has been deciphered from experimental data using elegant thermodynamic analyses.[22,30−32] Recently, Mg^{2+} triggered tertiary folding from preformed secondary structure has been studied by techniques including small angle diffraction,[6,33,34] time-resolved footprinting,[35,36] and a variety of single-molecule fluorescence techniques.[37−46] In addition, Mg^{2+} or protein or ligand-induced folding of a ribozyme,[47] retroviral kissing complexes,[48] rRNA elements,[49,50] and riboswitches[51,52] have been analyzed using optical tweezers. Two recent studies extended this approach to study folding thermodynamics of DNA and RNA hairpins under a variety of ionic conditions.[53,54]

The minimal kissing complex is one of the simplest tertiary interactions containing only two GC pairs formed between hairpin loops (Figure 1a, inset).[55] The RNA structure was discovered in the 5′ untranslated region of the Moloney murine leukemia virus and plays an important role in the dimerization initiation of the retroviral genomic RNAs.[56] Despite consisting of only two base pairs, this kissing complex shows remarkably stability. The kissing dimer forms in merely 150 mM monovalent salt in the absence of Mg^{2+}.[57] Since the structure contains no apparent cavity, cations must bind diffusely. In addition, given its size, the structure can only bind to a limited number of cations.

Received: May 22, 2013
Revised: June 25, 2013
Published: June 28, 2013

   dx.doi.org/10.1021/bi400646x | *Biochemistry* 2013, 52, 4991−5001

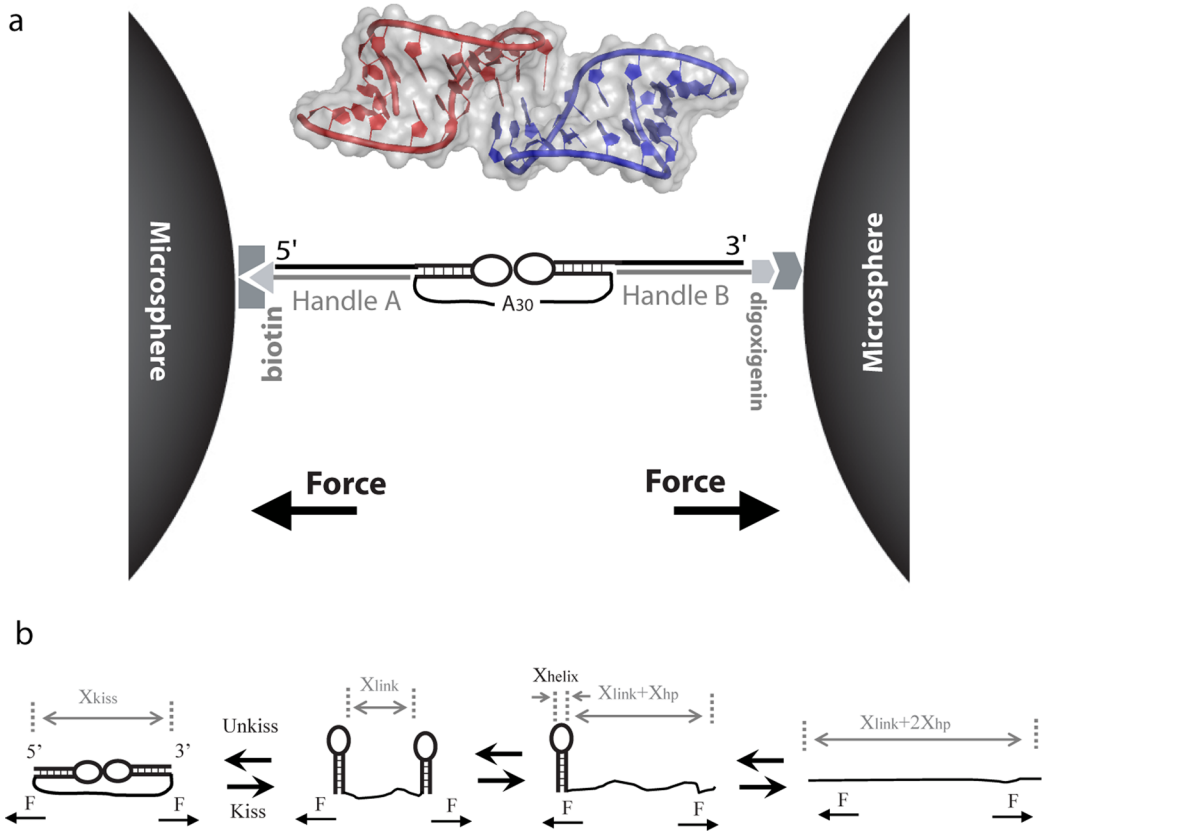

Figure 1. Mechanical unfolding of the minimal kissing RNA. (a) Experimental setup. The KC30 RNA was made of two RNA hairpins linked by 30 A-rich single-stranded nucleotides. Both hairpins had GACG loops, which could form a kissing complex of two GC base pairs.[59] The RNA was flanked by ~550 base double-stranded DNA-RNA handles. Through biotin-streptavidin and digoxigenin-antibody interactions, the entire molecule is tethered to two microspheres. Using optical tweezers, the RNA can be stretched and relaxed from its 5′- and 3′-ends.[60] Drawing is not to scale. Inset, NMR structure of the two-base-pair kissing complex.[55] (b) Unfolding and refolding pathways of the KC30 RNA.[59]

These features make the minimal kissing complex an attractive model to study diffuse ion binding to tertiary interaction.

The small size of the kissing complex, however, makes it difficult to study by UV melting, circular dichroism (data not shown), or gel mobility shift assay.[55,56] Previously, we developed a single-molecule mechanical unfolding assay to study the kissing complex, by which formation and breaking of the interaction can be directly observed.[57−59] In this work, we extended the optical tweezers based assay to evaluate the stabilizing effect of diffuse K^+ and Mg^{2+} ions on the kissing complex.

EXPERIMENTAL PROCEDURES

Preparation of RNA. The sequence of the KC30 RNA is 5′-CGGCGCUAGCAGACGUGCUAGCGCUGAAAAAUA-UCGAAAAAAAUACCAAAAAAAAACCUGGGAGACGUC-CCAGG-3′. The 30-nucleotide linker is underlined. The sequence was cloned into the pBR322 vector between *Eco*RI and *Hind* III sites. Detailed preparation of samples was described previously.[58−60] The synthesized KC30 RNA was flanked by two double-stranded DNA/RNA "handles", each of ~550 bases (Figure 1a). One end of the entire molecule had a biotin, and the other end was modified by a digoxigenin. The modifications allowed the molecule to be tethered between a pair of microspheres coated with streptavidin and anti-digoxigenin antibody, respectively.[60]

Mechanical Pulling Experiment. The mechanical pulling experiments were performed using a dual beam optical tweezers instrument.[61] The entire RNA molecule with handles was tethered between two microspheres in a flow chamber via noncovalent interactions (Figure 1a).[59] One bead was held by a force-measuring optical trap. The other microsphere was mounted on a micropipette. Moving the micropipette with a piezoelectric flexture stage changed the extension of the molecule, which in turn applied force on the molecule.[62] Force in picoNewtons (pN) and extension of the molecule in nanometer (nm) were recorded at a rate of 100 Hz. All pulling experiments were performed at 21 ± 0.5 °C at a rate of 5 pN/s using previously published protocols.[57,58,62,63] All solutions contained 10 mM HEPES, pH 8.0. In the Mg^{2+} titration experiments, all solutions contained 100 mM KCl and indicated concentrations of $MgCl_2$. HEPES acid and potassium salt, KCl, and $MgCl_2$ were purchased from Sigma.

RESULTS

Salt Effect on Mechanical Unfolding and Refolding Pathways. Mechanical unfolding of the KC30 RNA has previously been studied in 250 mM KCl.[59] The KC30 RNA follows hierarchical unfolding and folding pathways (Figure 1b). The breaking of the tertiary interaction, or the "unkissing", always occurs first, followed by unfolding of the two hairpins. In contrast, the hairpins refold before the formation of the kissing complex. On the force−extension curves (FEC), curves with a positive slope mainly reflects nonlinear elasticity of the double-stranded handles,[64] whereas the structural transitions are indicated by "rips" and "zips" with negative slopes.[75,79]

dx.doi.org/10.1021/bi400646x | *Biochemistry* 2013, 52, 4991−5001

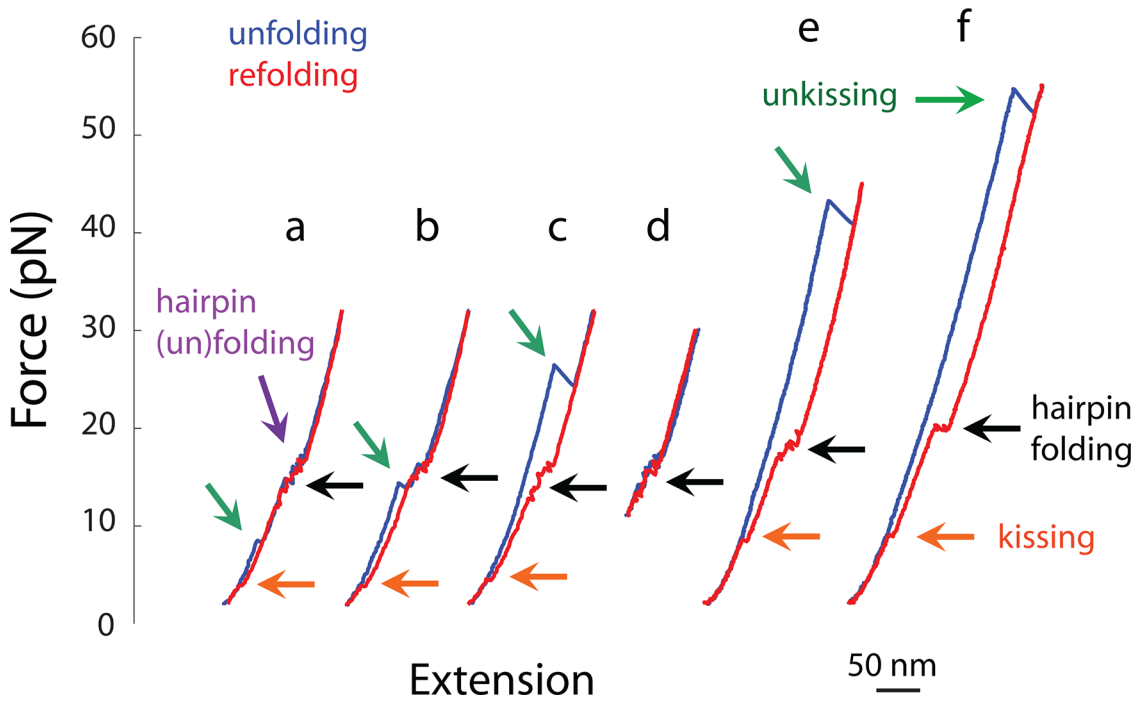

Figure 2. Force–extension curves of the KC30 RNA. (a–c) Three different types of trajectories observed in 100 mM KCl. (d) In a perturbation assay, the lowest force was set at 11 pN to prevent the kissing formation. (e) Folding in 1000 mM NaCl. (f) Folding in 100 mM KCl and 20 mM $MgCl_2$. Pulling curves are shown in blue and relaxation curves are in red. Structural transitions are indicated by colored arrows.

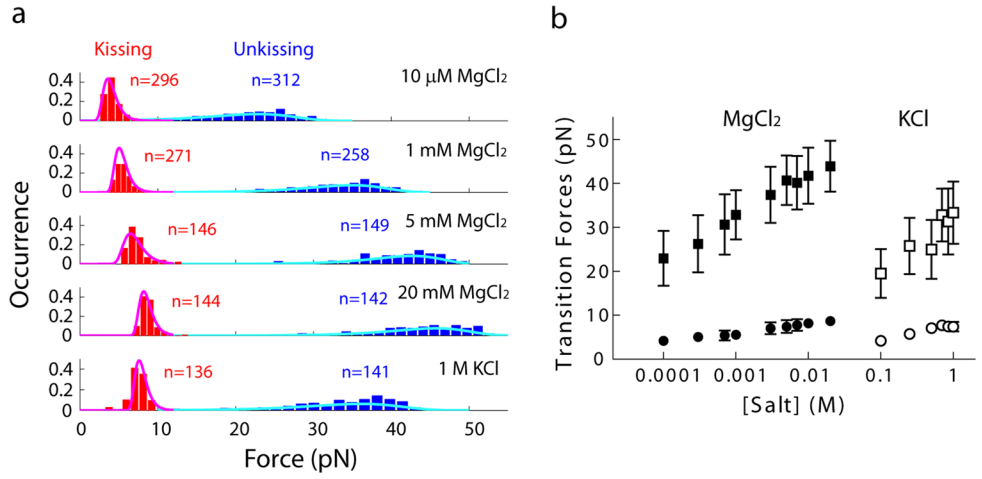

Figure 3. Salt effect on transition forces. (a) Distributions of the unkissing and kissing forces at selected salt concentrations. The colored curves were computed using eq 2 and extrapolated kinetic parameters from Table 1. (b) Unkissing (□ and ■) and kissing forces (○ and ●) as a function of KCl or $MgCl_2$ concentrations.

We performed pulling experiments on the KC30 RNA in various concentrations of KCl from 100 mM to 1 M, and in 100 mM KCl with concentrations of $MgCl_2$ varied from 10 μM to 20 mM. Under all tested conditions, each refolding trajectory of the RNA showed two classes of transitions (Figure 2, red curves). Hairpin folding was indicated by multiple back-and-forth transitions at 15–20 pN, reflecting bistability of the hairpin to single strand transitions at such forces.[60] A single zip at <12 pN suggested formation of a kissing interaction after folding of the hairpins. The sequence of refolding transitions was consistent with the proposed folding pathway (Figure 1b).

Upon unfolding, three types of trajectories were observed (Figure 2, blue curves). The three types of unfolding trajectories, however, reflect a single unfolding pathway (Figure 1b). The apparent difference in the FECs have been attributed to the fact that the unkissing occurs over a wide range of force, whereas the hairpins undergo structural transitions in a narrow force range.[59] If the unkissing occurs at lower forces than the unfolding of the hairpins, the trajectory shows three transitions (Figure 2a). The unkissing is characterized by a rip with small changes in extension (ΔX). As force is further raised, the two hairpins unfold. If the unkissing forces overlap with the unfolding forces of the hairpins, a "double-transition" is observed — the unkissing is followed immediately by unfolding of one of the two hairpins (Figure 2b). This double-transition has a larger ΔX than that of the unkissing alone. At slightly higher force, the second hairpin unfolds. If the kissing is unfolded at forces above those of the hairpins, most trajectories show a single rip with a large ΔX (Figure 2c). In this

dx.doi.org/10.1021/bi400646x | *Biochemistry* 2013, 52, 4991–5001

"triple-transition", both hairpins unfold only after the kissing interaction is broken. Since the hairpins are irreversibly unfolded at such high forces, the FECs showed no multiple back-and-forth transitions characteristic of reversible hairpin folding.

The three-step unfolding was mostly observed in solutions containing ≤250 mM KCl or <1 mM $MgCl_2$. As ionic strength increases, the unkissing occurred at higher force, and most trajectories displayed only a single rip (Figure 2e,f). The double-transitions occurred rarely under all experimental conditions.

To confirm this unfolding pathway, we performed a perturbation assay,[58,59] in which the RNA was relaxed to only 11 pN before pulling in order to prevent the kissing formation (Figure 2d). Subsequent pulling displayed only unfolding of the hairpins. This observation confirmed our assignments of the unkissing and kissing transitions. Furthermore, RNAs with mutations that disrupt the kissing interaction show similar trajectories as the ones observed in the perturbation assay.[57−59] By repeating the perturbation assay under different ionic conditions, we confirmed the assignments of the unkissing and kissing transitions. Therefore, the unkissing kinetics can be extracted from the first unfolding transition, whereas the kissing kinetics can be obtained from the last refolding transition. The different unfolding patterns affect unfolding of the hairpins but not the thermodynamics and kinetics of the kissing interaction.[59]

Salt Effects on Unkissing/Kissing Forces. The unkissing force shows a broad distribution as compared to the kissing force under each ionic condition (Figure 3a). From 0 to 20 mM Mg^{2+}, the unkissing forces showed a wide distribution over 20 pN, whereas the kissing forces fell in a range of less than 8 pN. Furthermore, widths of the unkissing and kissing force distributions were not significantly changed by salt concentrations. Interestingly, the average unkissing force increased faster with salt concentration than the kissing force (Figure 3b). For instance, the average unkissing force increased from 20.8 pN in 10 μM $MgCl_2$ to 43.9 pN in 10 mM $MgCl_2$, whereas the average kissing force changed from 4.3 pN to 8.7 pN under the same conditions. In 20 mM $MgCl_2$, some unfolding trajectories even showed unkissing transitions at >50 pN at a loading rate of 5 pN/s (Figure 2f), with the highest rip force observed at 54.7 pN. This is a surprisingly high force for breaking of merely two base pairs. As a comparison, unfolding and folding forces of the hairpins with 7- to 20-base-pair stems were raised by ∼5 pN under similar conditions (Figure 2).[53,54,65,66]

At >700 mM KCl or >5 mM $MgCl_2$, the unkissing and kissing forces remained largely unchanged with increasing salt concentration (Figure 3b), indicating saturated binding of cations to the two-base-pair structure. Interestingly, under saturated binding conditions, Mg^{2+} ions provided more stability to the tertiary structure than K^+. For example, the unkissing force in 20 mM $MgCl_2$ was ∼10 pN higher than that in 1 M KCl (Figures 2 and 3).

Kinetics Extracted from Force Distributions. From distributions of the transition forces, we determined the force-dependent unkissing and kissing kinetics using both Evans-Ritchie and Dudko methods (Figure S1, Supporting Information).[67,68] The Bell's kinetic model[69] was applied in the analyses to describe the a single activation barrier between folded and unfolded states:

$$k_F = k_0\, e^{FX^{\ddagger}/k_BT} \quad (1)$$

in which k_F is the rate constant at force F, k_0 is a factor reflecting both kinetics at zero force and instrumental effects, k_B is the Boltzmann constant, and T is the temperature in Kelvin, and $X^{\ddagger}$ is the distance from the folded/unfolded state to the transition states.[70] In previous works, the method worked reasonably well as evidenced by that kinetics obtained from pulling agrees with those from constant force measurement.[59] On the basis of the extrapolated force-dependent kinetics, the probability density function of transition forces at a loading rate r, $p(F)$, can be calculated from the following equation:[67]

$$p(F) = \frac{k_F}{r}\, e^{-\int_0^F (\frac{k_F}{r})\, df} \quad (2)$$

When superimposed on the force histogram, the computed $p(F)$ agreed with the distributions of transition force (Figures 3 and S1), validating the derived kinetics.

Salt Effect on Force-Dependent Kinetics. The tertiary unfolding and folding kinetics showed dependence on both force and ionic conditions (Table 1). At each ionic condition, the unfolding rate increased with force, whereas the kissing rate decreased when the force was raised (Figure 4). When the kinetics at two ionic conditions were compared, the unkissing rate in higher salt concentrations was lower, requiring higher forces to break the structure; the kissing kinetics and force increased by the addition of metal ions. Therefore, the stabilizing

Table 1. Unfolding and Refolding Kinetics under Various Ionic Conditions[a]

[KCl]	ln $k_{unfolding}$ (s^{-1})	$n_{unkissing}$[c]	ln $k_{refolding}$ (s^{-1})	$n_{kissing}$[c]
100 mM	$(0.193 \pm 0.006) \times F - (4.0 \pm 0.2)$	120	$(-1.49 \pm 0.04) \times F + (7.6 \pm 0.2)$	100
250 mM	$(0.172 \pm 0.003) \times F - (4.7 \pm 0.1)$	170	$(-1.4 \pm 0.1) \times F + (9.4 \pm 0.4)$	134
500 μM	$(0.155 \pm 0.004) \times F - (4.9 \pm 0.2)$	112	$(-1.59 \pm 0.05) \times F + (11.7 \pm 0.2)$	109
700 μM	$(0.194 \pm 0.006) \times F - (6.6 \pm 0.3)$	152	$(-1.36 \pm 0.05) \times F + (11.6 \pm 0.2)$	145
850 μM	$(0.147 \pm 0.006) \times F - (5.1 \pm 0.3)$	170	$(-1.47 \pm 0.04) \times F + (12.2 \pm 0.2)$	169
1000 mM	$(0.171 \pm 0.005) \times F - (6.1 \pm 0.1)$	141	$(-1.41 \pm 0.08) \times F + (12.4 \pm 0.5)$	136
[$MgCl_2$][b]				
10 μM	$(0.190 \pm 0.002) \times - (4.5 \pm 0.1)$	250	$(-1.26 \pm 0.05) \times F + (6.2 \pm 0.2)$	296
100 μM	$(0.189 \pm 0.003) \times F - (4.9 \pm 0.1)$	243	$(-1.24 \pm 0.02) \times F + (6.2 \pm 0.1)$	258
300 μM	$(0.199 \pm 0.006) \times F - (5.7 \pm 0.2)$	229	$(-1.30 \pm 0.02) \times F + (7.6 \pm 0.1)$	242
700 μM	$(0.178 \pm 0.007) \times F - (6.1 \pm 0.3)$	244	$(-1.21 \pm 0.01) \times F + (7.4 \pm 0.1)$	270
1 mM	$(0.204 \pm 0.003) \times F - (7.1 \pm 0.1)$	258	$(-1.34 \pm 0.03) \times F + (8.6 \pm 0.1)$	271
3 mM	$(0.187 \pm 0.005) \times F - (7.5 \pm 0.2)$	153	$(-1.09 \pm 0.06) \times F + (8.5 \pm 0.4)$	150
5 mM	$(0.23 \pm 0.01) \times F - (9.6 \pm 0.3)$	149	$(-0.89 \pm 0.09) \times F + (7.3 \pm 0.7)$	146
7 mM	$(0.192 \pm 0.006) \times F - (8.2 \pm 0.1)$	110	$(-0.99 \pm 0.07) \times F + (8.5 \pm 0.4)$	110
10 mM	$(0.182 \pm 0.003) \times F - (8.0 \pm 0.1)$	173	$(-1.28 \pm 0.02) \times F + (11.6 \pm 0.1)$	158
20 mM	$(0.208 \pm 0.004) \times F - (9.3 \pm 0.1)$	142	$(-1.32 \pm 0.06) \times F + (12.8 \pm 0.2)$	144

[a]The kinetics of the unimolecular unkissing/kissing is expressed in a transformed format of eq 1: ln $k_F = FX^{\ddagger}/k_BT$ + ln k_0, in which the slope is $X^{\ddagger}/k_BT$, and the y-intercept is ln k_0. [b]In titrating [$MgCl_2$], all solutions contained 100 mM KCl. [c]$n_{unkissing}$ and $n_{kissing}$ are numbers of observed transitions.

dx.doi.org/10.1021/bi400646x | Biochemistry 2013, 52, 4991−5001

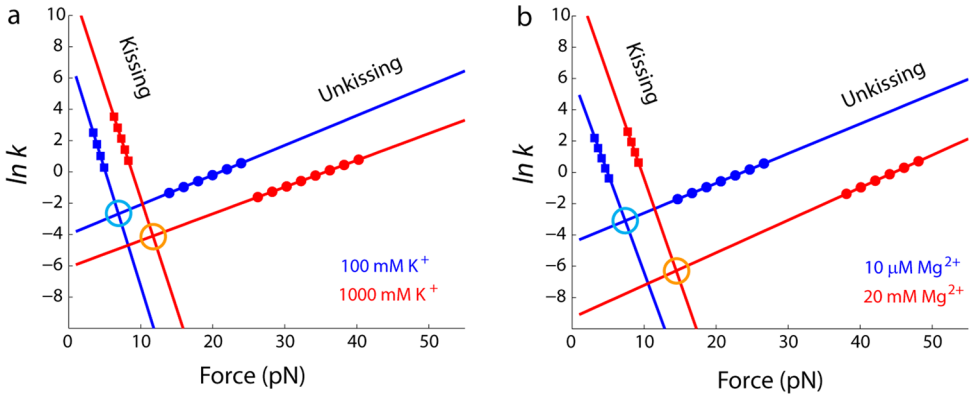

Figure 4. Salt effect on the unkissing and kissing kinetics. (a) Extrapolated kinetics in 100 mM (blue) or 1000 mM KCl (red). (b) Kinetics in 100 mM KCl with 10 μM (blue) or 20 mM $MgCl_2$. The symbol ● indicates the measured unkissing force within 1σ range, whereas ■ indicates the kissing force range. Open circles in light blue and orange were placed at the equilibrium points, at which forward and reverse rate constants are equal.

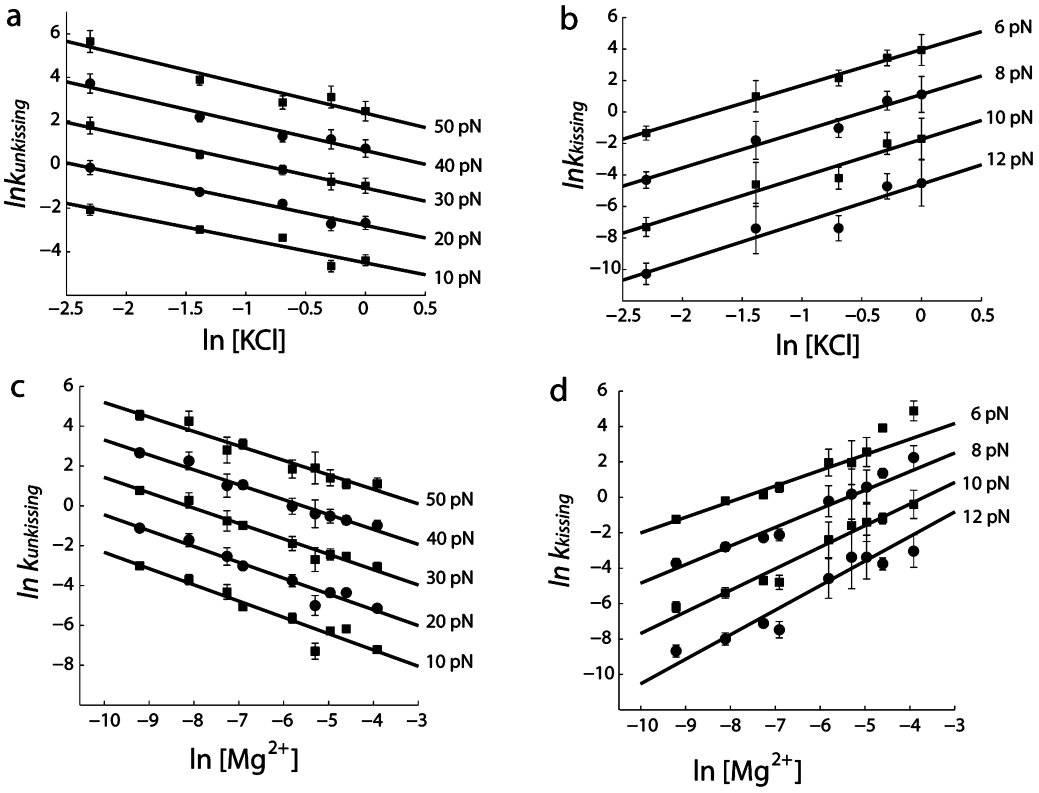

Figure 5. Folding kinetics as a function of salt concentration at selected forces. (a and b) ln $k_{unkissing}$ and ln $k_{kissing}$ as a function of K^+ concentration. (c and d) ln $k_{unkissing}$ and ln $k_{kissing}$ as a function of Mg^{2+} concentration. The solid lines are linear fits.

effect of metal ions arose from both slowing the dissociation and facilitating the association of the hairpins.

The slope of ln k vs F, which is $X^{\ddagger}/k_BT$ (eq 1), appeared to be similar under different ionic conditions (Figure 4 and Table 1). Under all tested conditions, $X^{\ddagger}_{unkissing}$ was 0.77 ± 0.08 nm, and $X^{\ddagger}_{kissing}$ was −5.3 ± 0.7 nm. As k_F increases exponentially with $X^{\ddagger}$, the larger value of $X^{\ddagger}_{kissing}$ resulted in fast increase of $k_{kissing}$ (Figure 4a). Consequently, the kissing formation occurred in a narrow range of force (Figure 3). In contrast, the smaller $X^{\ddagger}_{unkissing}$ was associated with slow increase of $k_{unkissing}$ and the broader distribution of the unkissing force. The relative salt independence of $X^{\ddagger}_{unkissing}$ and $X^{\ddagger}_{kissing}$ was consistent with the similar widths of transition force distributions under various ionic conditions (Figure 3). In contrast to $X^{\ddagger}$, ln k_0, the y-intercept on the ln k vs F plot, was significantly changed by metal ions. Therefore, the salt effect on the tertiary folding kinetics largely resulted from changes in k_0.

Mg^{2+} ions affected the kissing interaction more than K^+. As commonly seen in RNA folding,[71−74] a few millimolar of divalent metal ions had an equivalent stabilizing effect to monovalent cations in hundreds of mM (Table 1). Moreover, at their saturated binding, the stabilizing effect by Mg^{2+} ions was more pronounced than that by K^+. For example, the kinetics were similar in a solution containing 100 mM KCl with and without 10 μM Mg^{2+} (Figure 4, blue). Addition of 20 mM Mg^{2+} significantly decreased the unkissing kinetics, as compared to the effect by raising the concentration of KCl to 1000 mM (Figure 4, red).

***k_F* as a Function of Force and Salt Concentration.** To examine the salt effect on the kinetics at a constant force, we plotted ln k at selected forces as a function of salt concentration

dx.doi.org/10.1021/bi400646x | *Biochemistry* 2013, 52, 4991−5001

(Figure 5). At each force, both ln $k_{unkissing}$ and ln $k_{kissing}$ appeared to be a linear function of ln [salt]. The slope of ln $k_{unkissing}$ vs. [salt], $m^{\ddagger}_{unkissing}$, was −1.2 ± 0.1 for KCl and −0.8 ± 0.1 for $MgCl_2$. The $m^{\ddagger}_{kissing}$ was 2.4 ± 0.1 for KCl and 1.1 ± 0.2 for $MgCl_2$. The *y*-intercepts in each panel of the Figure 5 depended linearly on force (Figure S2). Because of the apparent linear dependence of the kinetics on the force and salt concentration, we attempted a first-order approximation to phenomenally describe the kinetics:

$$\ln k = \frac{FX^{\ddagger}}{k_B T} + \ln k_0 = \frac{X^{\ddagger}}{k_B T} \times F + m^{\ddagger} \times \ln[\text{salt}] + \ln k_{base} \quad (3)$$

in which ln k_{base} equal ln k_0 in the 1 M KCl data set, and at 100 mM KCl in the $MgCl_2$ data set. The ln k_0 in eq 1 can be expressed as ln $k_0 = m^{\ddagger} \times \ln[\text{salt}] + \ln k_{base}$. The entire KCl or $MgCl_2$ titration data were fitted to the eq 3:

$$\ln k_{unkissing,KCl} = (0.172 \pm 0.001) \times F - (1.2 \pm 0.1) \times \ln[KCl] + (-6.23 \pm 0.05) \quad (3a)$$

$$\ln k_{kissing,KCl} = (-1.42 \pm 0.01) + (2.4 \pm 0.1) \times \ln[KCl] + (12.51 \pm 0.01) \quad (3b)$$

$$\ln k_{unkissing,MgCl_2} = (0.223 \pm 0.001) \times F - (0.8 \pm 0.1) \times \ln[MgCl_2] + (-13.53 \pm 0.05) \quad (3c)$$

$$\ln k_{kissing,MgCl_2} = (-1.0 \pm 0.1) \times F + (1.1 \pm 0.2) \times \ln[MgCl_2] + (14.0 \pm 0.5) \quad (3d)$$

Such fitting agreed with data reasonably well (Figure S2). Also, the fitted values of $X^{\ddagger}$, $m^{\ddagger}$, and ln k_{base} were comparable to those from separate fits of ln *k* versus *F* (Figure 4) and ln *k* versus [salt] (Figure 5). This semiempirical treatment has also been applied to describe the unkissing kinetics of two six-base-pair kissing complexes[48] and the folding kinetics of a hairpin.[65] The eq 3 appears to be useful to describe the force and salt dependent kinetics of mechanical unfolding.

Δ*X* and Persistence Length of Single-Stranded RNA. Δ*X* of structural transitions observed on the FECs depend on both force and salt concentrations. The kissing interaction and the un/refolding of the hairpins occur in narrow force ranges (Figure 2); their Δ*X* can be compared with predicted values with relative ease.[57−59] Most unfolding transitions in this study were the triple-transitions, especially at medium and high salt concentrations. Interestingly, although the single-rips occurred over a force range >30 pN, $\Delta X_{single\text{-}rip}$ remained largely constant (Figure 6). The apparent dispersion of $\Delta X_{single\text{-}rip}$ was dominated by instrumental noises (Figure S3).

In a triple-transition, the kissing complex is unfolded into an extended single strand by the applied force (Figure 1b). The kissing complex under tension is assumed to be similar to the NMR structure,[55] in which the coaxially stacked helix-kissing-helix resembles a continuous helix. The end-to-end distance of 20-base-pair structure is 6 nm, much shorter than the persistence length of double-stranded RNA (>60 nm).[75] Therefore, the kissing complex can be treated as a rigid body whose extension is independent of force.[70,72] In contrast, the extension of the entire

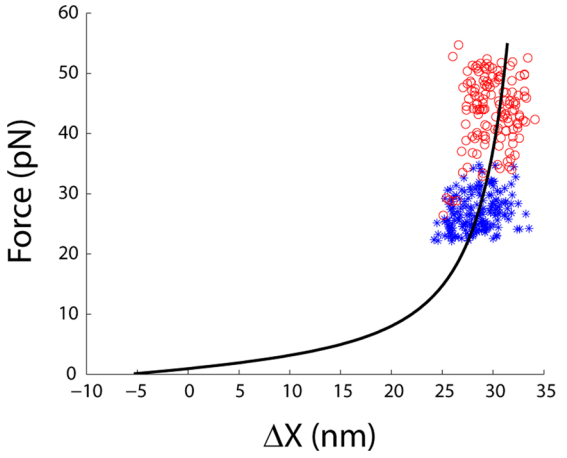

Figure 6. $\Delta X_{single\text{-}rip}$ as a function of the unkissing force. Symbols represent measured values in 100 mM KCl (blue *) or 20 mM (red ○) $MgCl_2$. The data superimposed on the worm-like-chain predictions (eq 4).

RNA in single-stranded conformation, X_{ss}, depends on the rip force *F*:[64]

$$F = \frac{k_B T}{P}\left[\frac{1}{4(1 - X_{ss}/L)^2} + \frac{X_{ss}}{L} - \frac{1}{4}\right] \quad (4)$$

in which *P* is the persistent length of the single strand, and *L* is its contour length. For single-stranded RNA, 1 and 0.59 nm per nucleotide are often used for persistence and contour lengths, respectively.[60,70,76]

Because $\Delta X_{single\text{-}rip}$ is the difference between the extensions of the two structures, changes in $\Delta X_{single\text{-}rip}$ are dominated by X_{ss}. We computed $\Delta X_{single\text{-}rip}$ as a function of force, which agreed with measured values (Figure 5). $\Delta X_{single\text{-}rip}$ increases slowly with force at >20 pN because the single-stranded RNA, already stretched to >75% of its contour length at such forces, cannot be much further extended.

The persistence length and the extension of a single-stranded RNA must be dependent on cationic conditions. However, this dependence has not been well characterized. On the basis of an energetic model, a recent study suggested that the persistence length of a single strand may decrease from 1.5 to 0.75 nm when the concentration of $MgCl_2$ increases from 10 μM to 10 mM.[54] Using these values, we predicted the difference in $<\Delta X_{single\text{-}rip}>$ under the two conditions to be ∼3 nm, significantly larger than the measured values (Figure 6). We have also observed similar salt concentration independence of $<\Delta X_{single\text{-}rip}>$ in the two other kissing complexes,[48] even though the three RNAs have different sizes and transition forces. The ionic effect on the extension of single-stranded RNA was perhaps less than that was reported.

Salt Effect on the Equilibrium of the Kissing Interaction. Mechanical unfolding of the kissing interaction is characterized by its irreversibility.[48,59] The irreversibility increased with ionic strength. Evidently, the gap between the unkissing and kissing forces enlarged as the salt concentration was raised (Figure 3). Hysteresis is observed even in the three-step unfolding trajectories under low salt conditions (Figure 2a), and increased significantly with salt concentration (Figure 2e,f). As a result, work dissipation, the difference between $work_{unkissing}$ and $work_{kissing}$, increased significantly with salt concentration (Figure 7a).

dx.doi.org/10.1021/bi400646x | *Biochemistry* 2013, 52, 4991−5001

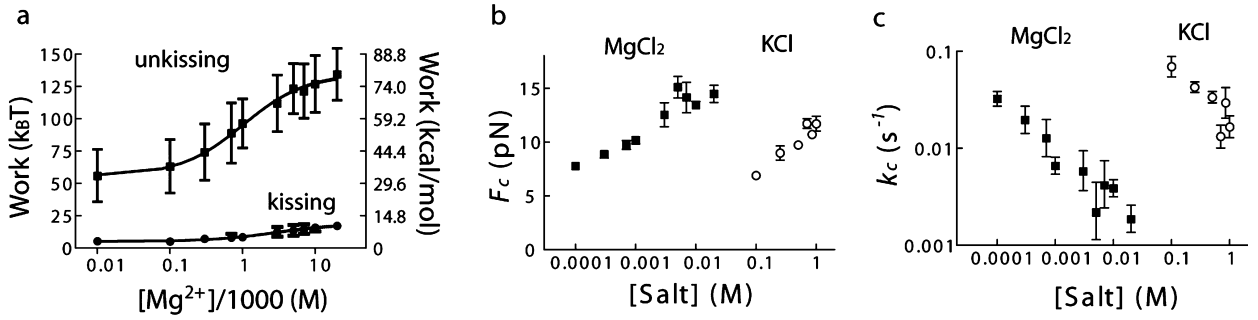

Figure 7. Equilibrium of the kissing interaction. (a) Mechanical work in the unkissing (■) and kissing (●) as a function of Mg^{2+} concentration. (b) F_c as a function of KCl (○) and $MgCl_2$ (■) concentrations. (c) k_c as a function of KCl (○) and $MgCl_2$ (■) concentrations.

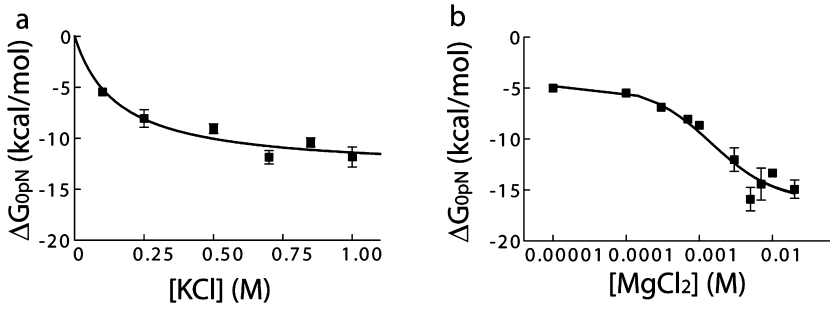

Figure 8. Folding free energy of the kissing complex at zero force. (a) ΔG_{0pN} as a function of KCl concentration. (b) ΔG_{0pN} as a function of $MgCl_2$ concentration. The curves represent fit to a single-site binding model.

To determine the equilibrium point, the apparent linear relation between ln k and F were extrapolated to the equilibrium force, F_c, at which $k_{unkissing}$ and $k_{kissing}$ are equal (Figure 4, ○).[70] The F_c increased with ionic strength (Figure 7b), suggesting that binding of metal ions stabilized the kissing complex. Such effect appeared to reach saturation at >700 mM KCl or in the presence of 100 mM KCl, at >5 mM $MgCl_2$. The F_c increased from 6.9 pN in 100 mM KCl to 11.7 pN in 1 M KCl, and from 7.4 pN in 10 μM $MgCl_2$ to 14.5 pN in 20 mM $MgCl_2$. The F_c at saturating $MgCl_2$ was ~3 pN higher than that at saturating KCl.

Interestingly, k_c, the rate constant at F_c, decreased with increasing salt concentrations (Figure 7c). The k_c decreased by ~4-fold from 100 mM to 1 M KCl, and by ~10-fold from 10 μM to 10 mM $MgCl_2$. In a study of folding an RNA hairpin,[65] we observed a similar trend that addition of salt increased hysteresis in the FECs and decreased k_c. Unlike the hysteresis, k_c is independent of pulling/relaxing rate. Hence, it is tempting to suggest that k_c can be used as an indicator of folding reversibility.

Thermodynamic Contributions by K^+ and Mg^{2+} Ions. The folding free energy of the kissing complex at the critical force, ΔG_{F_c}, equals the reversible mechanical work done to unfold the tertiary structure, i.e., $F_c \times \Delta X_{F_c}$.[66,76] When the kissing complex is unfolded into the conformation of the two linked hairpins (Figure 1b), the linker is stretched. To obtain folding free energy at zero force, ΔG_{0pN}, the stretching energy of the linker must be subtracted from the ΔG_{F_c}:

$$\Delta G_{0pN} = G_{F_c} - \text{work}_{linker} = F_c \times \Delta X_{F_c} - \int_0^{F_c} X_{linker}\, dF \quad (5)$$

in which the extension of the linker, X_{linker}, can be approximated by the worm-like-chain model (eq 4). In this work, we used a persistence length of 1 nm for all ionic conditions. We estimated that if the persistence length varies from 0.8 to 1.2 nm, the uncertainty of the stretching energy correction is <0.9 kcal/mol (or <8% of total ΔG) in the experimental range of F_c (Figure S4).

In 100 mM KCl, the kissing complex had a ΔG_{0pN} of −5.4 ± 0.3 kcal/mol. This negative value was consistent with the observations that hairpins can form stable dimers through the two-base-pair kissing interaction at low concentrations of monovalent salt.[55,57] The stabilizing effect of metal ions was shown by the significant decrease of ΔG_{0pN} as salt concentration was raised (Figure 8). At saturating Mg^{2+}, ΔG_{0pN} was ~−14 ± 1 kcal/mol, which was greater than that of ~−11.4 ± 0.8 kcal/mol at saturating K^+. The apparent K_d was ~160 mM for K^+ and 1.5 mM for Mg^{2+}, when fitted to a single site binding model.

DISCUSSION

Role of Metal Ions in the Apparent Unkissing and Kissing Kinetics. Both K^+ and Mg^{2+} ions stabilize the kissing complex by slowing unfolding and speeding up the refolding. The type and concentration of metal ions had relatively little effect on the force dependence of kinetics, described by $X^{\ddagger}/k_BT$ (eq 1), but significantly changed k_0 (Table 1 and Figure 4). In a simplified view, $X^{\ddagger}_{unkissing}$ and $X^{\ddagger}_{kissing}$ represent the distances from the unfolded and folded states to the barrier, respectively (Figure 9).[70] The salt independence of $X^{\ddagger}_{unkissing}$ and $X^{\ddagger}_{kissing}$ suggested that the position of the barrier along the reaction coordinate is not much altered by the metal ions. Instead, metal ions change the barrier height relative to the unfolded and folded states, as indicated by ln k_0.

As the effect of salt concentration was attributed to the k_0 but not $X^{\ddagger}$, the changes in the barrier height at each force, $\Delta\Delta G^{\ddagger} = k_BT \times (\ln k_2 - \ln k_1)$ (eq 3), were relatively force independent (Figure 4 and Table 1). For example, when the $MgCl_2$ concentration was raised from 10 μM to 1 mM to 20 mM, $\Delta\Delta G^{\ddagger}_{unkissing}$ increased by ~1.2 kcal/mol and ~1.1 kcal/mol,

dx.doi.org/10.1021/bi400646x | Biochemistry 2013, 52, 4991−5001

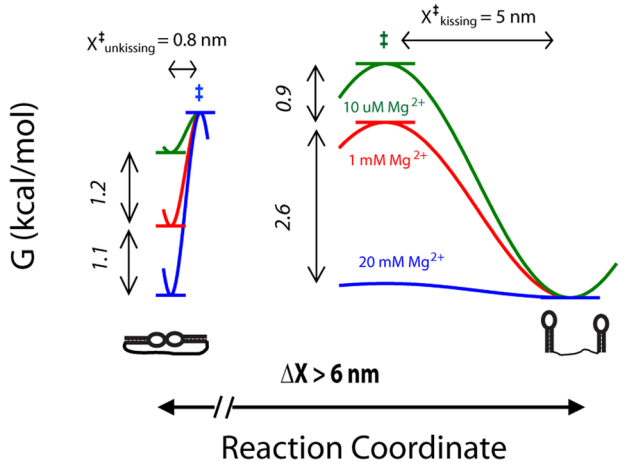

Figure 9. Energy landscape for mechanical unfolding of the kissing complex. The unkissing and kissing have different effective kinetic barriers. Increasing Mg^{2+} concentration from 10 μM (green) to 1 mM (red) to 20 mM increases the barrier heights but does not change the positions of the barriers along the reaction coordinate. The unkissing barrier and the two-hairpin conformation were arbitrarily superimposed for comparison.

respectively, whereas $\Delta\Delta G^{\ddagger}_{kissing}$ decreased by ~0.9 kcal/mol and ~2.6 kcal/mol, respectively (Figure 9).

Role of Metal Ions in a Two-Step Folding Model. Although both the unkissing and kissing appeared to occur in a single step (Figure 2), mechanical unfolding of the minimal kissing complex must have at least two substeps: the breaking/formation of the kissing base pairs, and extension/shortening of the single-stranded linker. In the unfolding, the rate-limiting step must be the disruption of the kissing base pairs, because it is energetically downhill to pull the two hairpins apart until the tension on the linker reaches the applied force.[59] Therefore, the transition state in the unkissing is likely to be a conformation that both kissing base pairs are just broken. Consistently, the measured $X^{\ddagger}_{unkissing}$ of ~0.8 nm indicates that the barrier in the unfolding is close to the folded state. This unfolding model is also supported by molecular dynamics simulations.[77] During kissing formation, the hairpins diffuse toward each other; at a close proximity, the loop−loop interaction forms. The large $X^{\ddagger}_{kissing}$ of ~5 nm suggests that the apparent barrier is affected by both the kissing base pairing and the intramolecular diffusion of the hairpins. Furthermore, if the folded and unfolded states are separated by a single kinetic barrier, the sum of $X^{\ddagger}_{forward}$ and $X^{\ddagger}_{reverse}$ equal ΔX. As demonstrated previously,[59] the sum of $X^{\ddagger}_{unkissing}$ and $X^{\ddagger}_{kissing}$ (<6 nm) was significantly shorter than ΔX (~8 nm at 7 pN, and ~11 nm at 15 pN), suggesting that there are different barriers in the unfolding and refolding.

The salt type and concentration affect both the kissing complex and the single-stranded linker. To estimate the ionic effect on the linker, we reanalyze published data of a mutant in which the two GACG tetraloops were replaced by GUCG.[57] The mutant RNA can form a pair of hairpins separated by a 30-nucleotide linker but not a kissing complex. By comparing the FECs of this RNA in 200 mM NaCl with those in 1 M NaCl and 20 mM $MgCl_2$, we estimated the energetic effect on the linker is less than 1.5 kcal/mol (Figure S5). This value, which is measured in a wider range of salt concentrations than the ones used in the work, is significantly smaller than the $\Delta\Delta G$ of the entire kissing complex (Figure 8). Therefore, it is safe to conclude that the observed $\Delta\Delta G_{ionic}$ of the KC30 RNA is attributed mostly to the kissing complex.

Differential Stabilizing Effects by K^+ and Mg^{2+}. The minimal kissing complex needs only very low concentrations of monovalent cations to form. However, its stability increases significantly with addition of K^+ and Mg^{2+}. Changes in the number of K^+ ions bound to the RNA upon kissing interaction, Γ_+, equals $m/2$, taking into account changes in both cation and anion concentrations.[78] Similarly, $\Gamma^{\ddagger}_{+,unkissing}$ and $\Gamma^{\ddagger}_{+,kissing}$ equal $m^{\ddagger}_{unkissing}/2$ and $m^{\ddagger}_{kissing}/2$, respectively. Since the experimental range of $MgCl_2$ was significantly lower than 100 mM Cl^- used in these experiments, Γ_{2+} and $\Gamma^{\ddagger}_{2+}$ can be approximated as m and $m^{\ddagger}$, respectively.

In kinetics, $\Gamma^{\ddagger}_{+,unkissing}$ of -0.6 ± 0.1 was similar to $\Gamma^{\ddagger}_{2+,unkissing}$ of -0.8 ± 0.1, whereas $\Gamma^{\ddagger}_{+,kissing}$ of 1.2 ± 0.1 and $\Gamma^{\ddagger}_{2+,kissing}$ of 1.1 ± 0.2 were statistically indistinguishable (Figure 5). Γ_{2+} of 3.1 ± 0.6 was larger than 1.9 ± 0.3, the sum of $\Gamma^{\ddagger}_{2+,unkissing}$ and $\Gamma^{\ddagger}_{2+,kissing}$. If the unfolded and folded states are separated by a single barrier, Γ_{2+} is equal to the sum of $\Gamma^{\ddagger}_{2+}$. This inequality between Γ_{2+} and the sum of $\Gamma^{\ddagger}_{2+}$ again suggested that the mechanical unfolding is more complicated than the two-state folding model. The Γ_+ of ~1.3 based on KCl titration is significantly lower than the sum of $\Gamma^{\ddagger}_{+,unkissing}$ and $\Gamma^{\ddagger}_{+,kissing}$. However, the value of Γ_+ is likely to be underestimated because the measurements were mostly taken at KCl concentrations higher than the apparent K_d of 160 mM (Figure 8a). The kissing complex formed in 50 mM KCl, as evident by the unkissing transitions in the FECs (data not shown). However, the kissing formations were not directly observed due to small ΔX at low forces, preventing thermodynamic determination under such conditions. Since the sum of $\Gamma^{\ddagger}_{+,unkissing}$ and $\Gamma^{\ddagger}_{+,kissing}$ is similar to that of the divalent metal ion, the actual value of Γ_+ is likely to be similar to Γ_{2+}. It is safe to conclude that folding and unfolding of the two-base-pair kissing complex is associated with uptake/expulsion of at least two and perhaps three diffuse K^+ or Mg^{2+} ions. Such estimations fell within the predicted range by the tightly bound ion model.[79] The similar values of Γ_+ and Γ_{2+} associated with the kissing interaction likely resulted from the fact that the limited size of the tertiary structure can only accommodate a finite number of counterions.

Interestingly, at their saturated binding, $F_{c,Mg^{2+}}$ was ~3 pN higher than F_{c,K^+} (Figure 7b); $\Delta G_{0pN,Mg^{2+}}$ was ~−2 kcal/mol lower than $\Delta G_{0pN,K^+}$ (Figure 8). The difference of metal ions was also reflected in the kinetics, particularly in the unfolding. The average unkissing force in saturated $MgCl_2$ was ~10 pN higher than that in saturated KCl (Figure 3). Consequently, FECs in 20 mM $MgCl_2$ displayed significantly larger hysteresis than those in 1000 mM KCl (Figure 2e,f). The k_c values at the two different conditions were different by almost 10-fold (Figure 7c). It is well-known that divalent Mg^{2+} ions are more effective in coordinating multiple phosphate groups than K^+. If the kissing complex binds to similar numbers of K^+ and Mg^{2+}, the divalent cations surely provide more stabilizing energy than the monovalent one.

Differential Salt Effects on the Unkissing and Kissing Forces. At first glance, the similar absolute values of $\Delta\Delta G^{\ddagger}_{unkissing}$ and $\Delta\Delta G^{\ddagger}_{kissing}$ between two salt concentrations were surprising (Figure 9). The similar values were in sharp contrast to differential changes in the unkissing and kissing forces. When the $MgCl_2$ concentration was raised from 10 μM to 20 mM, the average unkissing force was raised by 23 pN, and the average kissing force changed by merely 4.5 pN (Figure 3). This apparent paradox can be explained by that changes in transition forces, ΔF, depend on both $\Delta\Delta G^{\ddagger}$ and $X^{\ddagger}$:

dx.doi.org/10.1021/bi400646x | Biochemistry 2013, 52, 4991−5001

$$\Delta F = \Delta\Delta G^{\ddagger}/X^{\ddagger} \quad (6)$$

In the minimal kissing complex, $X^{\ddagger}_{\text{unkissing}}$ is ~0.8 nm and $X^{\ddagger}_{\text{kissing}}$ is ~5 nm. Between 10 μM Mg^{2+} and 20 mM Mg^{2+}, $\Delta\Delta G^{\ddagger}_{\text{unkissing}}$ of 2.3 kcal/mol increased the average unkissing forces by ~20 pN, whereas $\Delta\Delta G^{\ddagger}_{\text{kissing}}$ of 3.5 kcal/mol increased the average kissing forces by ~5 pN (Figure 9). This estimation agreed with observed transition forces (Figure 3).

Clearly, the salt dependent change of transition forces critically depends on $X^{\ddagger}$, which in turn depends on how force is applied to the molecular structure (Figures 1b and S6).[59] At the unfolding transition state, both kissing base pairs are broken by shearing forces, as evident by that the structure was extended by $X^{\ddagger}_{\text{unkissing}}$ of 0.8 nm (Figure 9) and by results from molecular dynamics simulations.[77] In contrast, the applied force is aligned with the single-stranded linker and the unkissed hairpins can rotate. The intramolecular diffusion under tension resulted in a large value of $X^{\ddagger}_{\text{kissing}}$. The difference in force-structure geometry contributed to the different values of $X^{\ddagger}_{\text{unkissing}}$ and $X^{\ddagger}_{\text{kissing}}$. It is possible to modulate $X^{\ddagger}$ and therefore, the sensitivity of the salt dependence by engineering the molecular structure relative to the applied force.[58]

Because the unkissing forces increased much faster with the salt concentration than the kissing forces, the tertiary folding become more irreversible, as evident by increased hysteresis in the FECs (Figure 2). The work dissipation in the tertiary folding, which was up to 32 kcal/mol or 130 k_BT (Figure 7a), is significantly larger than those seen in the secondary folding under similar conditions (usually less than 5 kcal/mol or 20 k_BT).[50,65] Because the unkissing is the rate-limiting first step, the hairpins could be unfolded at forces much higher than their F_c (Figure 2d,e). Hence, folding of the entire RNA dissipated even more work than the kissing interaction alone. The large values of work dissipation required an impractical number of observations to retrieve equilibrium free energy using the Jarzynski's equality theorem.[80−82] Instead, the folding free energy was computed by extrapolating forward and reverse kinetics to the equilibrium force (Figure 4).

The two-base-pair kissing complex is the weakest loop−loop interaction known to date and is difficult to detect by many equilibrium assays.[57] The irreversibility, however, manifests the tertiary folding and its binding to metal ions. Furthermore, specific signals of the tertiary folding distinctive from those of the secondary structure eliminate the need of signal deconvolution. The differential salt dependence of transition forces can be used to effectively detect metal ion binding, as evident by large changes in the unkissing force with salt concentrations. The magnitude of such changes depends on $X^{\ddagger}$, which in turn depends on the direction of applied force relative to the molecular bonds.

In vivo, RNA folding is affected by the ever-changing cellular ionic conditions, as various ion channels open and close frequently. In addition, RNA structure may change upon binding to metabolites, proteins, and other RNAs. These associations also depend on the ionic conditions. Given such complexity, the presence of two interacting domains may not always result in a tertiary contact. For example, formation of the intramolecular kissing complex in the cobalamin riboswitch requires 15 mM Mg^{2+} in the absence of the ligand; however, the kissing complex is observed at merely 0.5 mM Mg^{2+} in the presence of the metabolite.[83] This example manifests the importance of cations in the RNA folding and structure-mediated gene regulation. Knowledge of RNA−ation interaction is indispensable to our understanding of RNA biology. The technique developed in this study can be generally applied to study tertiary folding and its salt dependence.

■ ASSOCIATED CONTENT

Supporting Information

Methods to derive kinetics from distributions of transition forces, global fitting of kinetics, spatial resolution of the instrument, uncertainty in the stretching energy of the linker, and the physical meaning of $X^{\ddagger}$. This material is available free of charge via the Internet at http://pubs.acs.org.

■ AUTHOR INFORMATION

Corresponding Author

*Phone: 518-591-8879. Fax: 518-442-4767. E-mail: pli@albany.edu.

Funding

This work was supported by a National Science Foundation Grant MCB-1054449 and an IPRP grant from The RNA Institute at University at Albany.

Notes

The authors declare no competing financial interest.

■ ACKNOWLEDGMENTS

We thank Dr. Alan Chen and Mr. William Stephenson for suggestions and comments on the manuscript.

■ ABBREVIATIONS

FEC, force−extension curves; pN, picoNewton

■ REFERENCES

(1) Auffinger, P., Grover, N., and Westhof, E. (2011) Metal ion binding to RNA. *Met. Ions Life Sci. 9*, 1−35.
(2) Chen, S. J. (2008) RNA folding: conformational statistics, folding kinetics, and ion electrostatics. *Annu. Rev. Biophys. 37*, 197−214.
(3) Chu, V. B., Bai, Y., Lipfert, J., Herschlag, D., and Doniach, S. (2008) A repulsive field: advances in the electrostatics of the ion atmosphere. *Curr. Opin. Chem. Biol. 12*, 619−625.
(4) Draper, D. E. (2008) RNA folding: thermodynamic and molecular descriptions of the roles of ions. *Biophys. J. 95*, 5489−5495.
(5) Johnson-Buck, A. E., McDowell, S. E., and Walter, N. G. (2011) Metal ions: supporting actors in the playbook of small ribozymes. *Met. Ions Life Sci. 9*, 175−196.
(6) Pollack, L. (2011) SAXS studies of ion-nucleic acid interactions. *Annu. Rev. Biophys. 40*, 225−242.
(7) Lindahl, T., Adams, A., and Fresco, J. R. (1966) Renaturation of transfer ribonucleic acids through site binding of magnesium. *Proc. Natl. Acad. Sci. U. S. A. 55*, 941−948.
(8) Schimmel, P. R., and Redfield, A. G. (1980) Transfer RNA in solution: selected topics. *Annu. Rev. Biophys. Bioeng. 9*, 181−221.
(9) Pyle, A. M. (2010) The tertiary structure of group II introns: implications for biological function and evolution. *Crit. Rev. Biochem. Mol. Biol. 45*, 215−232.
(10) Woodson, S. A. (2010) Compact intermediates in RNA folding. *Annu. Rev. Biophys. 39*, 61−77.
(11) Strobel, S. A., and Cochrane, J. C. (2007) RNA catalysis: ribozymes, ribosomes, and riboswitches. *Curr. Opin. Chem. Biol. 11*, 636−643.
(12) Ferré-D'Amaré, A. R., and Winkler, W. C. (2011) The roles of metal ions in regulation by riboswitches. *Met. Ions Life Sci. 9*, 141−173.
(13) Smith, A. M., Fuchs, R. T., Grundy, F. J., and Henkin, T. M. (2010) Riboswitch RNAs: regulation of gene expression by direct monitoring of a physiological signal. *RNA Biol. 7*, 104−110.
(14) Roth, A. (2009) The structural and functional diversity of metabolite-binding riboswitches. *Annu. Rev. Biochem. 78*, 305−334.

(15) Steitz, T. A. (2008) A structural understanding of the dynamic ribosome machine. *Nat. Rev. Mol. Cell Biol. 9*, 242−253.
(16) Noller, H. F. (2005) RNA structure: reading the ribosome. *Science 309*, 1508−1514.
(17) Leung, E. K., Suslov, N., Tuttle, N., Sengupta, R., and Piccirilli, J. A. (2011) The mechanism of peptidyl transfer catalysis by the ribosome. *Annu. Rev. Biochem. 80*, 527−555.
(18) Mathews, D. H., Disney, M. D., Childs, J. L., Schroeder, S. J., Zuker, M., and Turner, D. H. (2004) Incorporating chemical modification constraints into a dynamic programming algorithm for prediction of RNA secondary structure. *Proc. Natl. Acad. Sci. U. S. A. 101*, 7287−7292.
(19) SantaLucia, J. J. (1998) A unified view of polymer, dumbbell, and oligonucleotide DNA nearest-neighbor thermodynamics. *Proc. Natl. Acad. Sci. U. S. A. 95*, 1460−1465.
(20) Cate, J. H., Gooding, A. R., Podell, E., Zhou, K., Golden, B. L., Kundrot, C. E., Cech, T. R., and Doudna, J. A. (1996) Crystal structure of a group I ribozyme domain: principles of RNA packing. *Science 273*, 1678−1685.
(21) Cate, J. H., and Doudna, J. A. (1997) A magnesium ion core at the heart of a ribozyme domain. *Nat. Struct. Biol. 4*, 553−558.
(22) Leipply, D., and Draper, D. E. (2011) Evidence for a thermodynamically distinct Mg2+ ion associated with formation of an RNA tertiary structure. *J. Am. Chem. Soc. 133*, 13397−13405.
(23) Das, R., Travers, K., Bai, Y., and Herschlag, D. (2005) Determining the Mg^{2+} stoichiometry for folding an RNA metal ion core. *J. Am. Chem. Soc. 127*, 8272−8273.
(24) Soto, A. M. M., V, and Draper, D. E. (2007) Tertiary structure of an RNA pseudoknot is stabilized by "diffuse" Mg^{2+} ions. *Biochemistry 46*, 2973−2983.
(25) Tan, Z. J., and Chen, S. J. (2011) Importance of diffuse metal ion binding to RNA. *Met. Ions Life Sci. 9*, 101−124.
(26) Kirmizialtin, S., and Elber, R. (2010) Computational exploration of mobile ion distributions around RNA duplex. *J. Phys. Chem. B 114*, 8207−8220.
(27) Bai, Y., Chu, V. B., Lipfert, J., Pande, V. S., Herschlag, D., and Doniach, S. (2008) Critical assessment of nucleic acid electrostatics via experimental and computational investigation of an unfolded state ensemble. *J. Am. Chem. Soc. 130*, 12334−12341.
(28) Bai, Y., Greenfeld, M., Travers, K., Chu, V. B., Lipfert, J., Doniach, S., and Herschlag, D. (2007) Quantitative and comprehensive decomposition of the ion atmosphere around nucleic acid. *J. Am. Chem. Soc. 129*, 14981−14988.
(29) Sharp, K. A., and Honig, B. (1995) Salt effects on nucleic acids. *Curr. Opin. Struct. Biol. 5*, 323−328.
(30) Leipply, D., and Draper, D. E. (2010) Dependence of RNA tertiary structural stability on Mg^{2+} concentration: interpretation of the Hill equation and coefficient. *Biochemistry 49*, 1843−1853.
(31) Lorenz, C., Piqaneau, N., and Schroeder, R. (2006) Stabilities of HIV-1 DIS type RNA loop-loop interactions in vitro and in vivo. *Nucleic Acids Res. 34*, 334−342.
(32) Weixlbaumer, A., Werner, A., Flamm, C., Westhof, E., and Schroeder, R. (2004) Determination of thermodynamic parameters for HIV DIS type loop-loop kissing complexes. *Nucleic Acids Res. 32*, 5126−5133.
(33) Behrouzi, R., Roh, J. H., Kilburn, D., and Woodson, S. A. (2012) Cooperative tertiary interaction network guides RNA folding. *Cell 149*, 348−357.
(34) Pollack, L., and Doniach, S. (2009) Time-resolved X-ray scattering and RNA folding. *Methods Enzymol. 469*, 253−268.
(35) Woodson, S. A. (2011) RNA folding pathways and the self-assembly of ribosomes. *Acc. Chem. Res. 44*, 1312−1319.
(36) Schlatterer, J. C., and Brenowitz, M. (2009) Complementing global measures of RNA folding with local reports of backbone solvent accessibility by time resolved hydroxyl radical footprinting. *Methods 49*, 142−147.
(37) Bokinsky, G., and Zhuang, X. (2005) Single-molecule RNA folding. *Acc. Chem. Res. 38*, 566−573.
(38) Joo, C., Balci, H., Ishitsuka, Y., Buranachai, C., and Ha, T. (2008) Advances in single-molecule fluorescence methods for molecular biology. *Annu. Rev. Biochem. 77*, 51−76.
(39) Hengesbach, M., Akiyama, B. M., and Stone, M. D. (2011) Single-molecule analysis of telomerase structure and function. *Curr. Opin. Chem. Biol. 15*, 845−852.
(40) Tinoco, I., Jr, and Gonzalez, R. L. J. (2011) Biological mechanisms, one molecule at a time. *Genes Dev. 25*, 1205−1231.
(41) Aitken, C. E., Petrov, A., and Puglisi, J. D. (2010) Single ribosome dynamics and the mechanism of translation. *Annu. Rev. Biophys. 39*, 491−513.
(42) Zhao, R., and Rueda, D. (2009) RNA folding dynamics by single-molecule fluorescence resonance energy transfer. *Methods 49*, 112−117.
(43) Blanchard, S. C. (2009) Single-molecule observations of ribosome function. *Curr. Opin. Struct. Biol. 19*, 103−109.
(44) Pljevaljcić, G., and Millar, D. P. (2008) Single-molecule fluorescence methods for the analysis of RNA folding and ribonucleoprotein assembly. *Methods Enzymol. 450*, 233−252.
(45) Solomatin, S. V., Greenfeld, M., Chu, S., and Herschlag, D. (2010) Multiple native states reveal persistent ruggedness of an RNA folding landscap. *Nature 463*, 681−684.
(46) Hodak, J. H., Downey, C. D., Fiore, J. L., Pardi, A., and Nesbitt, D. J. (2005) Docking kinetics and equilibrium of a GAAA tetraloop-receptor motif probed by single-molecule FRET. *Proc. Natl. Acad. Sci. U. S. A. 102*, 10505−10510.
(47) Onoa, B., Dumont, S., Liphardt, J., Smith, S. B., Tinoco, I., Jr, and Bustamante, C. (2003) Identifying kinetic barriers to mechanical unfolding of the T. thermophila ribozyme. *Science 299*, 1892−1895.
(48) Li, P. T., and Tinoco, I., Jr. (2009) Mechanical unfolding of two DIS RNA kissing complexes from HIV-1. *J. Mol. Biol. 386*, 1343−1356.
(49) Mangeol, P., Bizebard, T., Chiaruttini, C., Dreyfus, M., Springer, M., and Bockelmann, U. (2011) Probing ribosomal protein-RNA interactions with an external force. *Proc. Natl. Acad. Sci. U. S. A. 108*, 18272−18276.
(50) Collin, D., Ritort, F., Jarzynski, C., Smith, S. B., Tinoco, I., Jr, and Bustamante, C. (2005) Verification of the Crooks fluctuation theorem and recovery of RNA folding free energies. *Nature 437*, 231−234.
(51) Greenleaf, W. J., Frieda, K. L., Foster, D. A., Woodside, M. T., and Block, S. M. (2008) Direct observation of hierarchical folding in single riboswitch aptamers. *Science 319*, 630−633.
(52) Neupane, K., Yu, H., Foster, D. A., Wang, F., and Woodside, M. T. (2011) Single-molecule force spectroscopy of the add adenine riboswitch relates folding to regulatory mechanism. *Nucleic Acids Res. 39*, 7677−7687.
(53) Anthony, P. C. S., A Y, Chu, V. B., Doniach, S., Block, S. M., and Herschlag, D. (2012) Electrostatics of nucleic acid folding under conformational constraint. *J. Am. Chem. Soc. 134*, 4607−4614.
(54) Bizarro, C. V., Alemany, A., and Ritort, F. (2012) Non-specific binding of Na^{+} and Mg^{2+} to RNA determined by force spectroscopy methods. *Nucleic Acids Res. 40*, 6922−6935.
(55) Kim, C., and Tinoco, I. J. (2000) A retroviral RNA kissing complex containing only two G.C base pairs. *Proc. Natl. Acad. Sci. U. S. A. 97*, 9396−9401.
(56) D'Souza, V., Melamed, J., Habib, D., Pullen, K., Wallace, K., and Summers, M. F. (2001) Identification of a high affinity nucleocapsid protein binding element within the Moloney murine leukemia virus Psi-RNA packaging signal: implications for genome recognition. *J. Mol. Biol. 314*, 217−232.
(57) Stephenson, W., Asare-Okai, P. N., Chen, A. A., Keller, S., Santiago, R., Tenenbaum, S. A., Garcia, A. E., Fabris, D., and Li, P. T. X. (2013) The essential role of stacking adenines in a two-base-pair RNA kissing complex. *J. Am. Chem. Soc. 135*, 5602−5611.
(58) Li, P. T. X. (2013) Formation of a metastable intramolecular RNA kissing complex by nanomanipulation. *Soft Matter 9*, 3246−3254.
(59) Li, P. T. X., Bustamante, C., and Tinoco, I., Jr. (2006) Unusual Mechanical Stability of A Minimal RNA Kissing Complex. *Proc. Natl. Acad. Sci. U. S. A. 103*, 15847−15852.

(60) Liphardt, J., Onoa, B., Smith, S. B., Tinoco, I., Jr, and Bustamante, C. (2001) Reversible unfolding of single RNA molecules by mechanical force. *Science 292*, 733−737.
(61) Smith, S. B., Cui, Y., and Bustamante, C. (2003) Optical-trap force transducer that operates by direct measurement of light momentum. *Methods Enzymol. 361*, 134−162.
(62) Li, P. T. X., Collin, D., Smith, S. B., Bustamante, C., and Tinoco, I., Jr. (2006) Probing the Mechanical Folding Kinetics of TAR RNA by Hopping, Force-Jump and Force-Ramp Methods. *Biophys. J. 90*, 250−260.
(63) Li, P. T. X., Bustamante, C., and Tinoco, I., Jr. (2007) Real-time control of the energy landscape by force directs the folding of RNA molecules. *Proc. Natl. Acad. Sci. U. S. A. 104*, 7039−7044.
(64) Bustamante, C., Marko, J. F., Siggia, E. D., and Smith, S. B. (1994) Entropic elasticity of lambda-phage DNA. *Science 265*, 1599−1600.
(65) Stephenson, W., Keller, S., Santiago, R., Albrecht, J. E., Asare-Okai, P. N., Tenenbaum, S. A., Zuker, M. and Li, P. T. X. Combining temperature and force to study folding of an RNA hairpin. Submitted.
(66) Tinoco, I. J., Collin, D., and Li, P. T. X. (2004) The effect of force on thermodynamics and kinetics: unfolding single RNA molecules. *Biochem. Soc. Trans. 32*, 757−760.
(67) Dudko, O. K., Hummer, G., and Szabo, A. (2008) Theory, analysis, and interpretation of single-molecule force spectroscopy experiments. *Proc. Natl. Acad. Sci. U. S. A. 105*, 15755−15760.
(68) Evans, E., and Ritchie, K. (1997) Dynamic strength of molecular adhesion bonds. *Biophys. J. 72*, 1541−1555.
(69) Bell, G. I. (1978) Models for the specific adhesion of cells to cells. *Science 200*, 618−627.
(70) Tinoco, I., Jr, Li, P. T. X., and Bustamante, C. (2006) Determination of ther modynamics and kinetics of RNA reactions by force. *Q. Rev. Biophys. 39*, 325−360.
(71) DeRose, V. J. (2003) Metal ion binding to catalytic RNA molecules. *Curr. Opin. Struct. Biol. 13*, 317−324.
(72) Draper, D. E. (2004) A guide to ions and RNA structure. *RNA 10*, 335−343.
(73) Pyle, A. M. (2002) Metal ions in the structure and function of RNA. *J. Biol. Inorg. Chem. 7*, 679−690.
(74) Woodson, S. A. (2005) Metal ions and RNA folding: a highly charged topic with a dynamic future. *Curr. Opin. Chem. Biol. 9*, 104−109.
(75) Abels, J. A., Moreno-Herrero, F., van der Heijden, T., Dekker, C., and Dekker, N. H. (2005) Single-molecule measurements of the persistence length of double-stranded RNA. *Biophys. J. 88*, 2737−2744.
(76) Li, P. T. X., Vieregg, J., and Tinoco, I., Jr. (2008) How RNA unfolds and refolds. *Annu. Rev. Biochem. 77*, 27.1−24.
(77) Chen, A. A., and Garcia, A. E. (2012) Mechanism of enhanced mechanical stability of a minimal RNA kissing complex elucidated by non-equilibrium molecular dynamics simulations. *Proc. Natl. Acad. Sci. U. S. A. 109*, 1530−1539.
(78) Record, M. T., Jr., Zhang, W., and Anderson, C. F. (1998) Analysis of effects of salts and uncharged solutes on protein and nucleic acid equilibria and processes: a practical guide to recognizing and interpreting polyelectrolyte effects, Hofmeister effects, and osmotic effects of salts. *Adv. Protein Chem. 51*, 281−353.
(79) Tan, Z. J., and Chen, S. J. (2009) Predicting electrostatic forces in RNA folding. *Methods Enzymol. 469*, 465−487.
(80) Ritort, F., Bustamante, C., and Tinoco, I. J. (2002) A two-state kinetic model for the unfolding of single molecules by mechanical force. *Proc. Natl. Acad. Sci. U. S. A. 99*, 13544−13548.
(81) Jarzynski, C. (1997) Nonequilibrium equality for free energy differences. *Phys. Rev. Lett. 78*, 2690−2693.
(82) Liphardt, J., Onoa, B., Smith, S. B., Tinoco, I., Jr, and Bustamante, C. (2002) Equilibrium information from nonequilibrium measurements in an experimental test of Jarzynski's equality. *Proc. Natl. Acad. Sci. U. S. A. 296*, 1832−1835.
(83) Johnson, J. E., Jr., Reyes, F. E., Polaski, J. T., and Batey, R. T. (2012) B12 cofactors directly stabilize an mRNA regulatory switch. *Nature 492*, 133−137.